TIARA-REP-WP6-2012-015

Test Infrastructure and Accelerator Research Area

Status Report

Specifications for the new SLS beam size monitor: Deliverable 6.2

Milas, N. (PSI) *et al*

24 August 2012

The research leading to these results has received funding from the European Commission under the FP7-INFRASTRUCTURES-2010-1/INFRA-2010-2.2.11 project TIARA (CNI-PP). Grant agreement no 261905.

This work is part of TIARA Work Package **6: SVET R&D Infrastructure**.

The electronic version of this TIARA Publication is available via the *TIARA web site* at `http://www.eu-tiara.eu/database` or on the *CERN Document Server* at the following URL: `http://cdsweb.cern.ch/search?p=TIARA-REP-WP6-2012-015`

TIARA/WP6:SVET D_SPEC

Specifications for the new SLS beam size monitor

Natalia Milas, Martin Rohrer, Angela Saa Hernandez, Volker Schlott, Andreas Streun, Paul Scherrer Institute, Switzerland
Åke Andersson, Jonas Breunlin, MaxLab, Sweden

August 16, 2012

A new beam size monitor is going to be build in SLS in the context of the TIARA-WP6 collaboration. In the first section of this report the need of a new beam size monitor is justified, the main characteristics and improvements over the old one are listed, and the basic design is explained. In the second section several synchrotron radiation simulations studying the resolution for different wavelengths, different measuring methods, and the influence of alignment errors and surface errors on the toroidal mirror are presented. In the third section we present a plan for the beam line commission strategy. Then, in the fourth and fifth sections, the resulting specifications on the different optical and mechanical elements are listed. Finally, in the sixth section, the schedule for the installation and commissioning of the new beamline is provided. The existing instrumentation of the SLS storage ring was already described in the interim report [1] and has not been included.

1 The new beam size monitor - Concept and basic design

The π-polarization method enables the measurement of the beam size by imaging the vertically polarized vis-UV synchrotron radiation [2]. A sketch of the measurement principle is shown in Figure 1. The electron beam circulating through the dipole generates synchrotron radiation. The radiation in the range of x-rays has a small opening angle and is obstructed before reaching the mirrors by a horizontal obstacle also known as *finger absorber*. Also the horizontally polarized radiation on the vis-UV range, heavily concentrated in the mid-plane, is partly obstructed by the finger absorber. Thus, mainly vertically polarized radiation travels along the beamline, where it is focused either by a lens or by a toroidal mirror on a CCD camera situated at the image plane. At the CCD camera the two lobes of the π-polarized radiation, which have a phase difference of 180°, are then imaged showing the characteristic destructive interference at the mid-plane. For a point-like beam, this interference is complete and the central intensity is zero. Instead, for an extended source a non-zero valley intensity is observed. The ratio of the valley-to-peak intensity can be related to the source size and, in this manner, it is possible to infer the beam size, and from it the beam emittance.

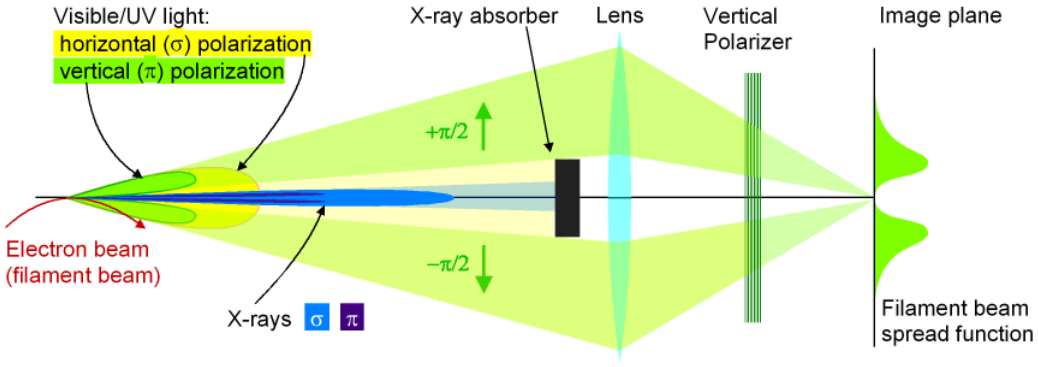

Figure 1: Sketch of the π-polarization measurement principle.

The new beamline will be located at the central dipole of sector 8 (BX08), which is the only dipole with free space after the SLS concrete shield. In order to avoid x-ray and bremsstralung, the beamline has been designed following a zigzag shape which ensures that only UV-visible radiation can reach the exit aperture. A simplified layout of the design of the new beamline is shown in Figure 2. The central out-coupling port will be used due to its larger vertical acceptance for the synchrotron light. However, further modifications of the absorbers of dipole BX08 are necessary, modifications on the same line as the ones that already took place in the current beam size montior beamline.

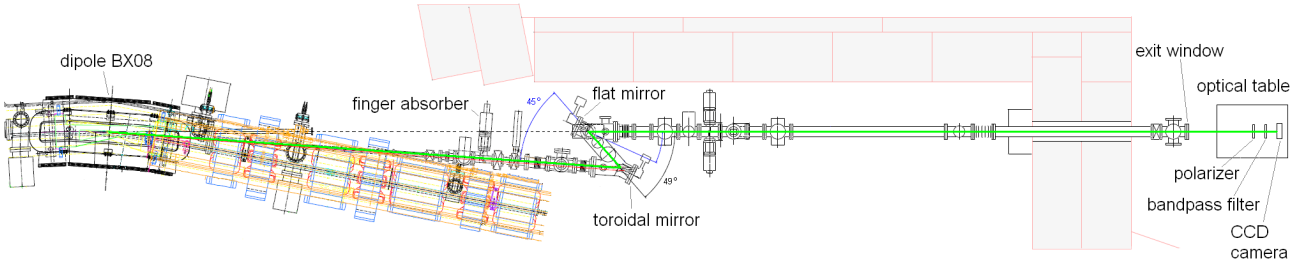

Figure 2: Simplified layout of the new beam size montior beamline.

1.1 Why is a new monitor necessary?

The vertical emittance minimization campaign at SLS realized in the context of the TIARA WP6 [3] has already achieved the world's smallest vertical beam size, $\sigma_y = 3.6 \pm 0.6$ μm, and vertical emittance, $\varepsilon_y = 0.9 \pm 0.4$ pm, in a synchrotron light source [4]. The minimum value reached for the vertical emittance is only about five times bigger than the quantum limit $\varepsilon_y = 0.2$ pm [5]. However, the resolution limit of the present monitor has also been reached during this campaign, thus, to further continue the emittance minimization program the construction of an improved second monitor is necessary.

The main characteristics, and subsequent improvements, of the new monitor will be:

- Longer beamline that will end outside the SLS tunnel. As a consequence the optical table will be full-time accessible, also during machine operation.
- Higher magnification ratio, $M = -1.45$, approximately a factor two higher than for the old monitor, which will increase the measurement precision.
- Wavelength-independent monitor, build exclusively with reflective elements, which will enable the use of different wavelengths without the necessity of a realignment of the image plane. To this end, the focusing element will be a toroidal mirror instead of a lens. Anyhow, the design of the new beamline includes a port for a lens, such that it could be included as a fall-back option.,
- Possibility to use shorter wavelengths, which will increase the sensitivity to smaller beam sizes. For example, by lowering the measured wavelength from 364 nm to 266 nm the limit of the monitor is driven from 3.5 μm to 2.7 μm.
- Availability of a set of vertical obstacles with different heights (15, 20 and 25 mm) to enable the interferometric measurement method, which will increase the sensitivity to smaller beam sizes and provide an additional measurement method to cross-check the results.

In Figure 3 a schematic representation of the new and the old beamline designs are presented for comparison.

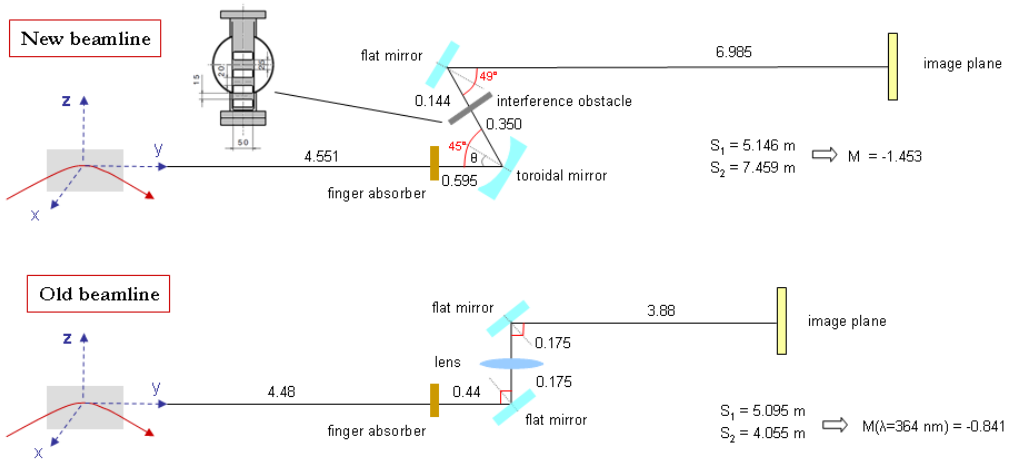

Figure 3: Comparison between the new (top) and old (bottom) beam size montior beamlines.

2 Simulations and expected performance

The results from an extensive investigation of the expected performance of the beam size montior under the influence of different sources of errors are presented in this section. The sim-

ulations of the synchrotron radiation propagation along the new beamline have been performed using the SRW (Synchrotron Radiation Workshop) code [7].

2.1 Resolution

2.1.1 Resolution as a function of the wavelength

The new beam size montior will be wavelength independent, which means that the focal length, and thus the image plane, will be situated at the same position independent of the wavelength of the detected radiation. For this reason, different wavelengths in the range vis-UV can be chosen for imaging the beam size, being the selection of wavelength only limited by the availability of commercial bandpass filters of the desired bandwidth.

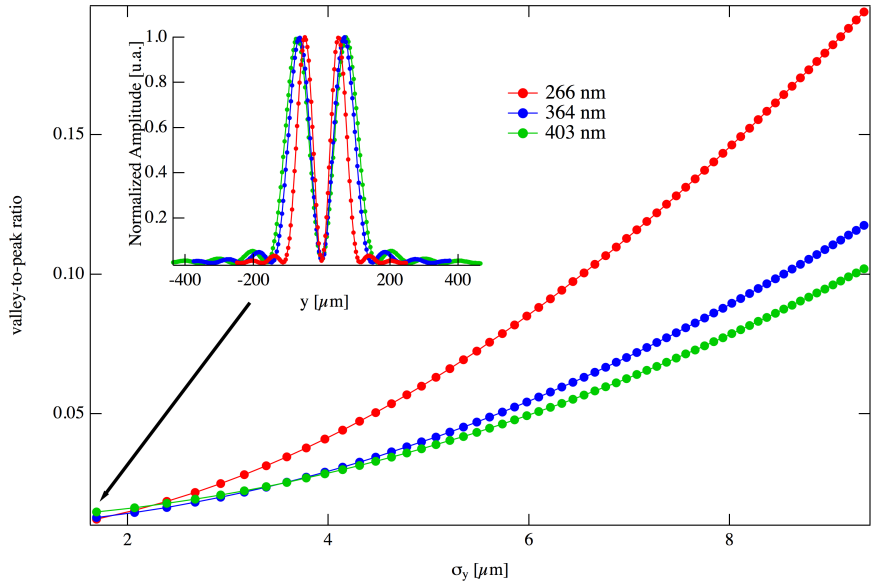

Figure 4: Valley-to-peak ratios as a function of the beam size for different wavelengths. The inset plot shows the vertically polarized light profile for the smallest vertical beam size. The sampling of the profiles is simulating a CCD camera with a pixel size of 3.75 μm, which shows that the number of sampling points is enough to resolve the peaks and valleys even for very small beam sizes.

The valley-to-peak intensity ratio is plotted in Figure 4 as a function of the beam size for three different wavelengths. For shorter wavelengths it is easier to resolve the beam size as the slope of the curve is steeper, thus increasing the sensitivity of the valley-to-peak intensity.

The inset plot in Figure 4 shows the profile of the π-polarized light for the three different wavelengths, sampled at intervals of 3.75 μm. As shown, an additional consequence of the detection of shorter wavelengths is an increase of the proximity of the two peaks. However, in contrary to the old monitor, the new monitor will not be limited in wavelength due to a poor

resolution when peaks go closer. This is due to the new CCD camera with a pixel size of 3.75 μm, which together with a magnification of $M = -1.45$ ensures enough sampling points to resolve peaks and valleys for wavelengths down to 266 nm.

2.1.2 Resolution as a function of the measurement method: imaging versus interferometric methods.

The beam size montior will work in two different modes: pure imaging and inference. The intensity distribution of the vertically polarized light and the corresponding image at the CCD camera for the two modes can be compared in figure 7.

In the pure imaging mode, also called π-polarized mode, an image of the two lobes from the π-polarized light is made, and the height ratio of the valley to the peaks (I_{valley}/I_{peak}) is used as an indirect measurements of the vertical beam size. In this mode, in addition to the beam height and width it is also possible to extract information from the local vertical dispersion by measuring the tilt in the image on the CCD camera. Further details on this method can be found in [2].

Although its several advantages, the resolution of the π-polarized method is limited for very small beam sizes (4 μm or less), as the sensitivity of this method to beam height changes becomes weak for smaller values. In order to gain sensitivity to small beam sizes we can make use of the interferometric method [6], by introducing a double slit in front of the light beam. The principle of this measurement is called the *van Cittert-Zernike theorem*, and is based on the fact that a measurement of spatial coherence of synchrotron light in the vis-UV region is related to the beam size.

The synchrotron radiation interferometer is a double slit interferometer using polarized quasi-monochromatic light. When the light intensities at the two slits are the same (i.e. once the beam is symmetrically positioned with respect to them), the interference pattern at the detector plane can be written as:

$$I(y) = I_0 \left[\mathrm{sinc}\left(\frac{2\pi a}{\lambda R}y + \phi\right)\right]^2 \left[1 + \gamma \cos\left(\frac{2\pi D}{\lambda R}y + \psi\right)\right] \tag{1}$$

where I_0 is the light intensity through the slits, a is the slit width, R is the distance between the source and the slits, D is the double slit separation, λ is the wavelength, γ the visibility measured at the double slit separation D, ϕ and ψ are phase shifts. In our case the first phase term ϕ in equation 1 is not relevant, it describes diffraction effects on the slits and since we have just an obstacle, i.e. $a >> \lambda$, those effects are negligible. The second phase term, on the other hand, is import and it will differentiate the fringe pattern observed and the fit function for the σ ($\psi_\sigma = \psi$) or π ($\psi_\pi = \psi + \pi$) polarized radiation. The term $\psi = \tan^{-1}(S(D)/C(D))$, where $S(D)$ and $C(D)$ are the sine and cosine components of the Fourier transformation of the distribution function of the synchrotron radiation source.

In case of a gaussian beam distribution (using σ-polarized light) this measurement is quite

simple, and the RMS beam size is given by:

$$\sigma_y = \frac{\lambda R}{\pi D M}\sqrt{\frac{1}{2}\ \ln\left(\frac{1}{\gamma}\right)} \quad \text{with} \quad \gamma = \left(\frac{I_{max} - I_{min}}{I_{max} + I_{min}}\right) \tag{2}$$

where M is the beamline magnification and I_{max} and I_{min} the intensities of the peaks and valleys in the interferogram.

Figure 5 shows the visibility for σ-polarized light with a vertical beam size of 2 μm as the double slit separation and the detected wavelength are varied. The values for the slit separation in the new beamline will be 15, 20 and 25 mm. Simulations were done for the three double-slit separations combined with wavelengths of 266, 364 and 403 nm. Based on the experience of other laboratories [6] and with the available equipment we expect to be able to distinguish a visibility of 0.97 from one of 0.95, assuming an error bar around 0.01 for the visibility. Thus, we would have enough range to measure beam sizes as small as 2 μm.

It is possible to compare the resolution of the π-polarized method with the interferometric method (also for the vertically polarized light) if the value for the visibility is rearranged as: $I_{peak}/I_{valley} = (1+\gamma)/(1-\gamma)$. From the simulation we can show that, assuming the same sensitivity for the new beamline as the one for the old beamline, we can resolve beam sizes of the order or 2 μm, in agreement with the calculation and limitations also shown before.

A disadvantage of the interferometer method is that beam rotations, which would indicate the presence of spurious vertical dispersion, would be obscured by the fringe pattern.

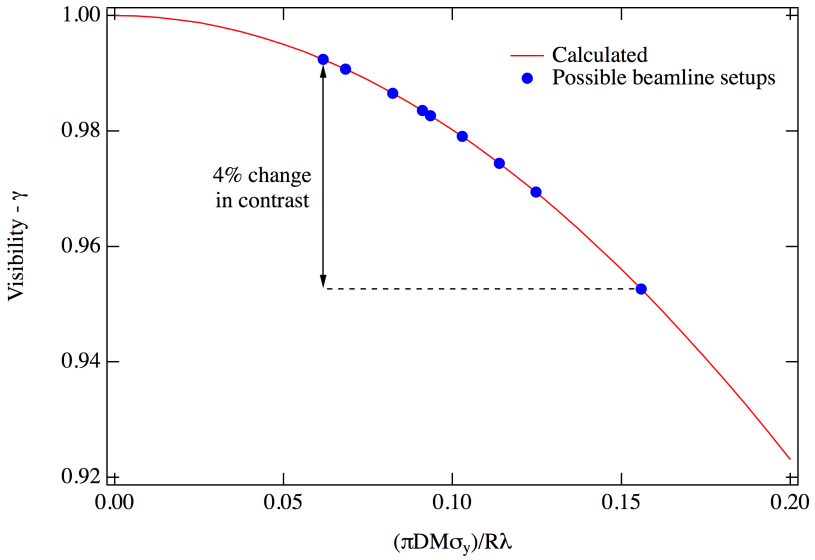

Figure 5: Calculated visibility for σ-polarized light for a vertical beam size of 2 μm. It is foreseen for this beamline to have three different slits separations sizes (15, 20 and 25 mm) and also to work at multiple wavelengths. In the plot we show possible measurements for the three double-slit separations combined with wavelengths of 266, 364 and 403 nm.

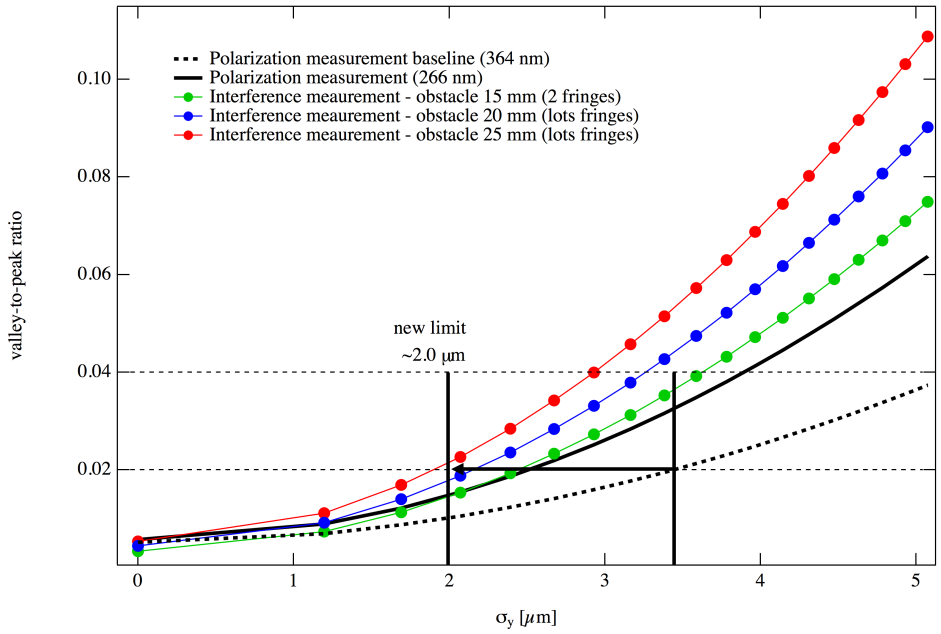

Figure 6: Simulated visibility of the vertically polarized light as a function of vertical beam size for the π-polarized method and the interferometer method with the three available obstacles.

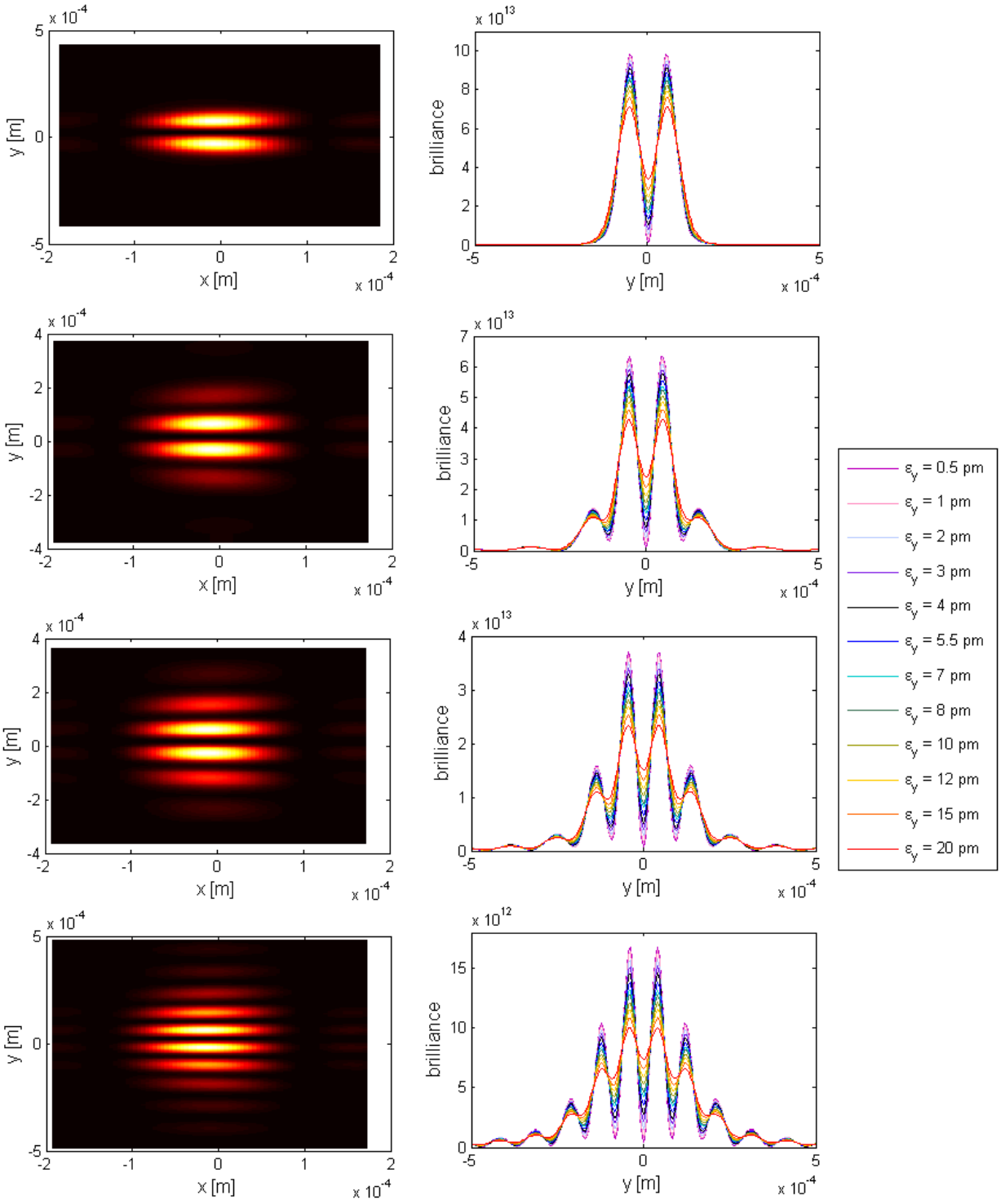

Figure 7: Vertically polarized light for the different measurement methods; the π-polarization (top) and the interferometric method with the three different obstacle widths: 15 mm (2^{nd} row), 20 mm (3^{rd} row) and 25 mm (bottom). On the right column the corresponding vertical projection represented for different vertical emittances.

2.2 Misalignments and rotation of the toroidal mirror

The toroidal mirror will be mounted over a gimbal mount, a pivoted support which allows the rotation of the mirror about the horizontal and vertical axis while keeping its center fixed. In order to define the constraints on mechanical alignment and beam positioning necessary to resolve beam sizes as small as 2 μm, all possible misalignments of the toroidal mirror from its ideal position have been included in the SRW simulations. The results of these simulations are also aimed to guide us during the beamline commissioning phase, as some misalignments result in a characteristic image at the CCD camera.

Five alignment errors have been considered:

D_x Horizontal offset
D_y Vertical offset
T_x Horizontal tilt
T_y Vertical tilt
R Rotation around mirror axis

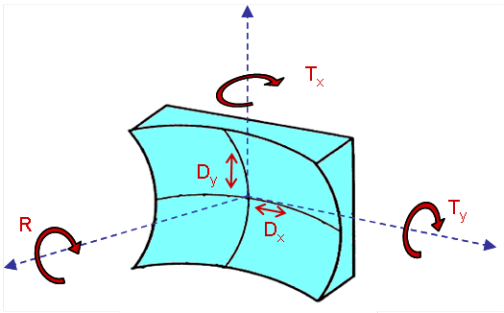

A summary of the valley-to-peak ratio as a function of the different alignment errors is represented in Figure 8. In the left plot the valley-to-peak ratio is represented as a function of the horizontal or vertical offset of the toroidal mirror. In the right plot the valley-to-peak ratio is represented as a function of the tilt around the horizontal, vertical or normal axis of the mirror. In a dashed line is plotted the valley-to-peak value an ideally aligned mirror would have.

In the subsequent sections we discuss the effect for each of the possible errors and we define the constraints on mechanical alignment and beam positioning necessary to be able to resolve beam sizes as small as 2 μm.

2.2.1 Offsets

The gimbal mount does not provide any translational degree of freedom, that is, possible horizontal and vertical offsets of the beam from the center of the mirror would not be compensated by the mount and could only be adjusted by varying the beam orbit.

Simulations of the propagation of synchrotron radiation along a beamline with horizontal or vertical offsets of the toroidal mirror have been run in SRW. The results show an offset, correspondingly scaled, of the detected radiation at the image plane. However, both the horizontal and the vertical offsets conserve the valley-to-peak ratio of the image at the CCD camera, as shown for the vertical projection in figure 9. Thus, it can be concluded that an offset of the toroidal mirror is harmless for the determination of the beam size.

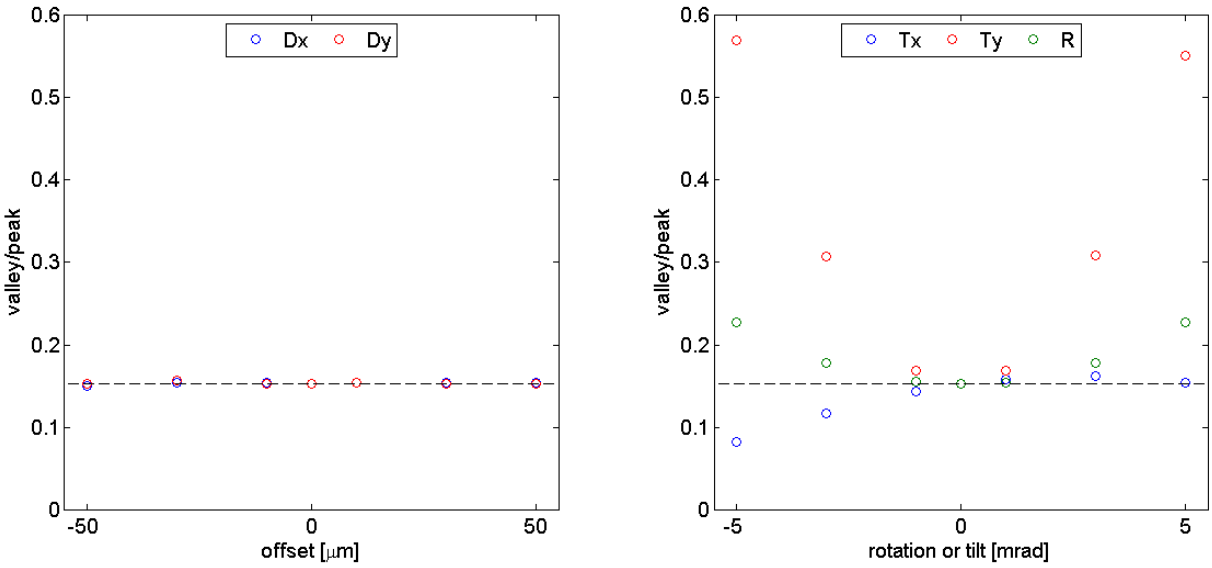

Figure 8: Valley-to-peak ratio as a function of the different misalignment; as a function of the horizontal and vertical offsets (left) and as a function of the horizontal and vertical tilts and the rotation around the mirror normal axis (right).

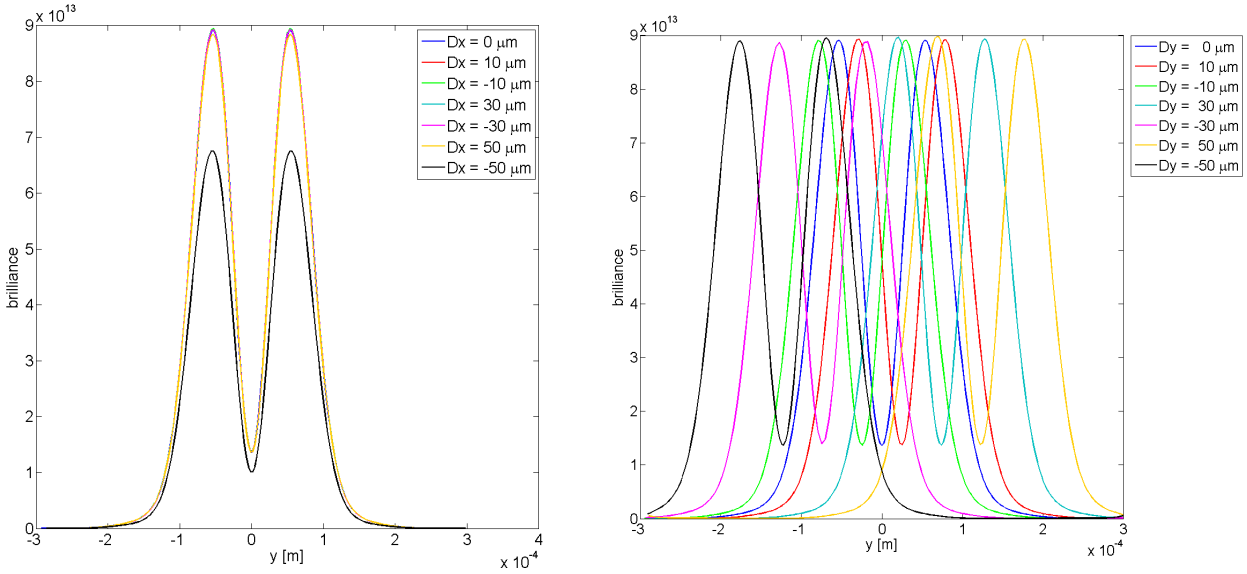

(a) Horizontal offset

(b) Vertical offset

Figure 9: Vertical projection of the vertically polarized light detected at the camera for different offsets of the toroidal mirror. SRW simulation corresponding to a beam of $\sigma_y = 9$ μm.

2.2.2 Tilts

The gimbal mount provides two rotational degrees of freedom and it can be used to compensate tilts around the horizontal and the vertical axes.

A vertical tilt of the toroidal mirror is equivalent to a change of the vertical incident angle from the nominal normal incidence. As a result the horizontal and vertical focusing planes are mixed. The simulations along a beamline with a vertically tilted toroidal mirror show an asymmetry of the intensity distribution of the synchrotron radiation detected at the CCD camera. This asymmetry can be observed in the vertical projection and distorts the valley-to-peak ratio symmetrically for the mirror being tilted in one or the other direction, as shown in Figure 10b In this case, the estimation of the beam size from the valley-to-peak measured ratios would be very overestimated (by 11%, 100% and 270% for tilts of $\pm$ 1 mrad, $\pm$ 3 mrad, and $\pm$ 5 mrad, respectively), as shown in Figure 8. To avoid an overestimation of the beam size the vertical tilt will be compensated by adjusting the gimbal mount until a symmetric peak pattern is observed at the camera.

A horizontal tilt of the toroidal mirror is equivalent to a change of the horizontal incident angle from the nominal 22.5° between the beamline and the mirror normal. In this case there is no mixing between planes, but the simulations show changes in the intensity distribution of the synchrotron radiation due to the geometry variation. These changes in the intensity distribution affect the measured valley-to-peak ratio, as shown in Figure 10a. The effect is not symmetric for the mirror being tilted in one or the other direction. In this case, the estimation of the beam size from the valley-to-peak measured ratios would be underestimated for tilts decreasing the incident angle (by 6%, 33% and 46% for tilts of -1 mrad, -3 mrad, and -5 mrad, respectively), and overestimated for tilts increasing the incident angle (by 4%, 6% and 1% for tilts of 1 mrad, 3 mrad, and 5 mrad, respectively), as shown in Figure 8. To avoid an underestimation of the beam size the horizontal tilt will be compensated by adjusting the gimbal mount until the distance between the two peaks is minimum.

2.2.3 Rotation

The gimbal mount does not provide a rotational degree of freedom around the mirror normal axis, and thus cannot compensate this type of misalignment. A toroidal mirror has a different radius in the horizontal and vertical planes. Thus, a rotation around the normal axis results in a different focal length for the horizontal and vertical planes and generates astigmatism (the horizontal and vertical image planes are situated at different positions). The simulations along a beamline with a toroidal mirror rotated around the normal axis show an asymmetry of the intensity distribution of the synchrotron radiation detected at the CCD camera. This asymmetry can be observed in the vertical projection and distorts the valley-to-peak ratio symmetrically for the mirror being rotated in one or the other direction, as shown in Figure 11. As a result of the distorted measurements of the valley-to-peak ratios the beam size would be overestimated by 1.5%, 17% and 49% for a toroidal mirror rotated by $\pm$ 1 mrad, $\pm$ 3 mrad, and $\pm$ 5 mrad, respectively, as shown in Figure 8.

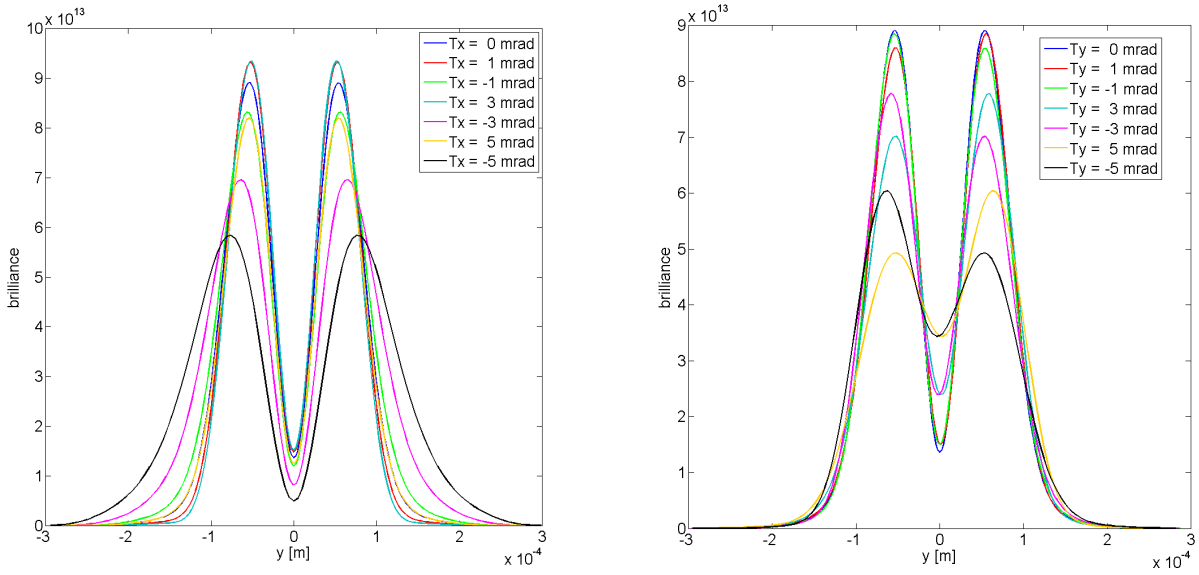

(a) Horizontal tilt

(b) Vertical tilt

Figure 10: Vertical projection of the vertically polarized light detected at the camera for different tilts of the toroidal mirror. SRW simulation corresponding to a beam of $\sigma_y = 9$ μm. In Figure (a) all the curves overlap expect those for $/pm$ 50 μm, where intensity is reduced due to shadowing of the SR light on one of the apertures of the beamline.

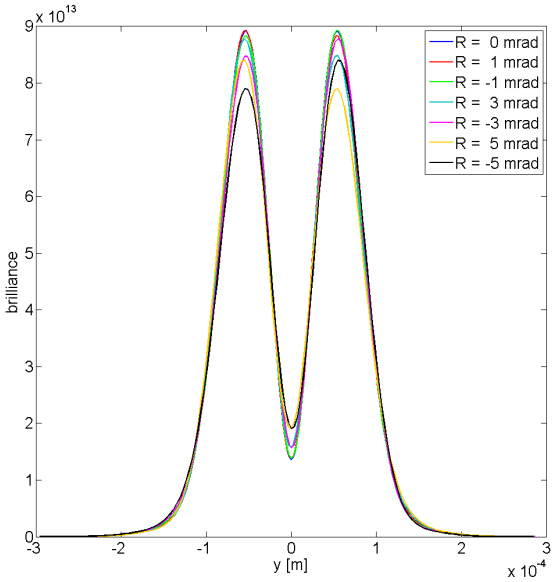

Figure 11: Vertical projection of the vertically polarized light at the camera for a toroidal mirror rotated around its axis. SRW simulation corresponding to a beam of $\sigma_y = 9$ μm.

As the effect of a rotation around the mirror normal axis affects the beam size estimation and as it cannot be compensated realigning the gimbal mount, the consequences of this alignment error

are studied in more detail. In Figure 12 the expected error on the valley-to-peak ratio is shown for different rotation errors. According to the simulation the mirror rotation has to be ≤ 1 mrad, values which are feasible according to the PSI alignment group and the mechanical design of the mount. We expect thus, that the contribution of rotation error on the determination of the beam size to be ≤ 0.1 μm, i.e., less than 5% of the beam size.

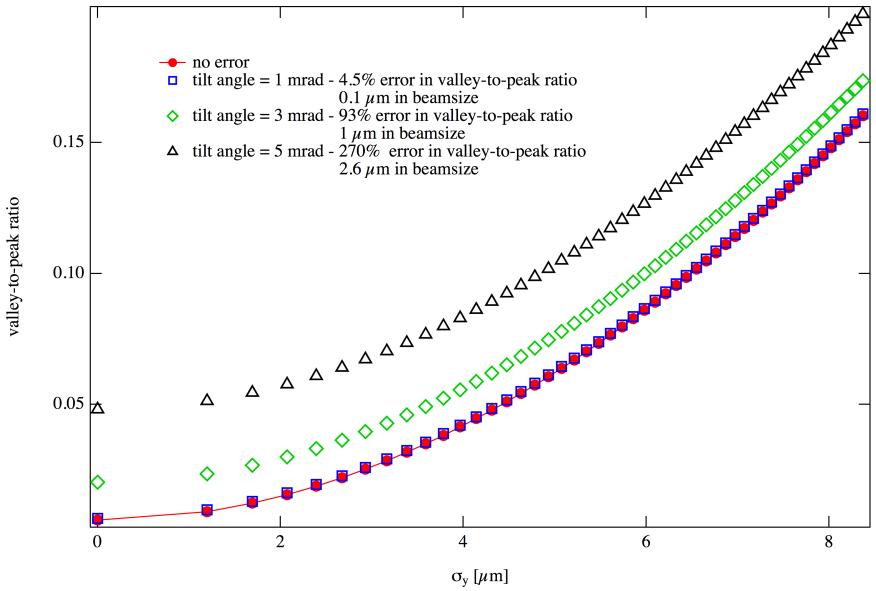

Figure 12: Calibration curve of peak-to-valley ratio for three different rotation errors of the toroidal mirror: 1, 3 and 5 mrad. The simulations are run for a beam with vertical size of 2 μm, for which the effect is the biggest. In order to be able to resolve beam sizes as small as 2 μm the mirror has to be aligned with a precision better than 1 mrad with respect to the beam central orbit plane.

2.3 Mirror surface quality

The aberrations or distortions produced by an optical element on the image plane are not only caused by the alignment errors, but are also affected by the imperfections and texture of its surface. Thus, a reliable description of the optical elements is essential for having accurate simulations of the synchrotron radiation propagation along the beamline. As the surface imperfections prevent the reflected rays to meet at one unique point on the image plane, thus producing a blurred image, such simulations are necessary during the design process in order to set the specifications and tolerances of the optical elements to be produced. Afterwards, once the optical elements have been produced and the measured profiles are available, it is desirable to include them in the simulations for a more realistic description of the beamline.

In this section it is presented the generation of a realistic surface profile for the toroidal mirror following the model from [8]. Afterwards, the results of the synchrotron radiation simulations including a non-ideal toroidal mirror are discussed and the tolerances for the manufacturers are

set.

The imperfections of the surface of an optical element can be classified into three families: roughness, waviness and geometry errors.

Roughness is a random irregularity with an average period in the range of ångströms. The surface roughness depends on the finishing process and the mechanical properties of the materials.

Waviness is the ripple of the surface shape. The spatial period of the ripple lies between few mm and hundreds of μm, and is a function of the polishing process used in the final manufacture.

Geometry error is a deformation of the macroscopic curvature of the surface, produced by thermal loads and mechanical stress.

To simulate a realistic surface profile for the toroidal mirror we have implemented the model developed by [8], based on the idea that the surface waviness can be simulated by a series of sine or cosine signals having the frequencies which are multiples of the fundamental $(2L)^{-1}$, related to the length L of the surface. Afterwards the surface roughness, which is randomly generated, is added to the surface waviness. A surface profile generated using this model is represented in figure 13. In this case the amplitude of the first harmonic is set to zero, which means that no deformation of the macroscopic curvature is included. The waviness has been generated by including ten harmonics (from the second harmonic to the eleventh) with randomly generated amplitudes, initial phases and coherent lengths. Finally, the surface roughness, generated randomly following a gaussian distribution with a mean value of 0 nm and a RMS value of 1 nm, has been been superposed.

The surface texture cannot be included in the definition of the mirror element in SRW. Instead it is included as a plane just behind the mirror that defines its transmission pattern, thus modifying the path length of the light in the same manner as the surface texture would do it. In a mirror the path length variation occurs twice due to reflection.

The surface errors of the mirror cause a peak asymmetry in the image observed at the CCD camera. A separated analysis of waviness and roughness shows that the effect of the roughness is negligible, at least for a surface roughness with an RMS value up to 2 nm, while the waviness is fully responsible for the observed effects. For this reason specifications have to be set on the maximum height difference (*maximum peak-to-valley*) and slope variations (*slope error*) tolerable for the toroidal mirror.
There is an additional parameter of the waviness which seems to play a key role; the orientation of the waves or surface ripples. The orientation of the waves depends on the polishing process performed on the mirror. Thus, for a polishing with circular movements the surface presents a

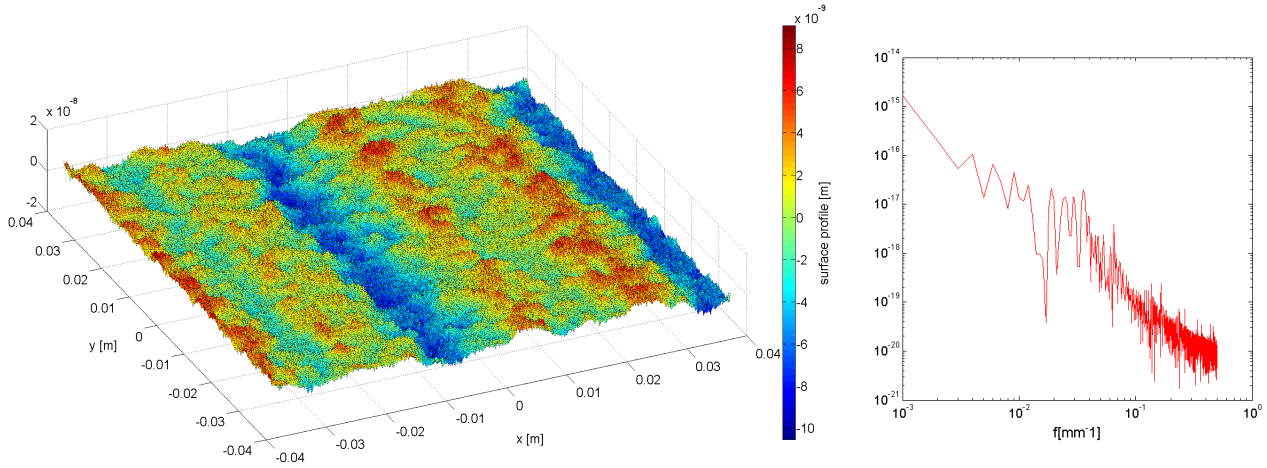

Figure 13: Simulated surface profile of the toroidal mirror (left) and corresponding PSD function (right).

radial waviness pattern (this is usually the case for the lenses), while for a polishing with linear movements it presents a horizontal or vertical striped pattern. As shown in figure 14, the peak asymmetry is more pronounced for the horizontally striped pattern than for the radial or the vertically striped pattern. This effect seems to be purely geometrical; in the case of a surface with horizontal waves the two lobes of vertically polarized light hit various crests and valleys of neighboring stripes and the path length of the two light lobes is modified in a different manner. Instead, in the case of a surface with vertical waves the two lobes of vertically polarized light hit the same stripe, thus suffering a much smaller path length variation. In this case the small peak asymmetry observed is due to the small path length variation produced by the roughness and the small bumps within a stripe. For a mirror with radial waves the two lobes of vertically polarized light will hit approximately symmetric areas of the mirror, as long as the mirror is correctly aligned and there is a negligible vertical offset. All the required specifications for the mirror manufacturers are listed in section 4.1.

In order to prove the independence of the focusing element on the peak asymmetry produced by the surface errors, the same surfaces were included on a beamline using a lens instead of a toroidal mirror. The results of the simulations show exactly the same relation of peak asymmetry.

3 Commissioning strategy

In order to be able to align the toroidal mirror, instead of using SR radiation at the very beginning we decided to use a known source, which would make the alignment simpler. The

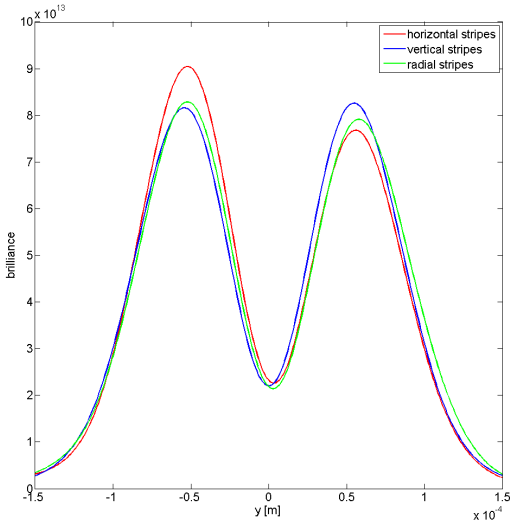

Figure 14: vertical projection of the vertically polarized light for a toroidal mirror with different patterns of surface waviness.

plan is then to use a UV-laser (wavelength between 250 and 400 nm) with a set of symmetric and non-symmetric pinholes. In the bemaline a motorized mirror just before the finger absorber can be inserted in order to shot the laser through a fused silica window and along the same path followed by the synchrotron light. The laser, a set of different pinholes sizes and shapes and some motorized mirrors will be fixed to a breadboard and then installed inside of the tunnel at the same distance as the SR source. Using a pinhole we can find the optical plane (focus) of the beamline and correct horizontal tilt, since it influences the horizontal and vertical focal planes differently. Using a asymmetric pinhole (with which any mixing of vertical and horizontal profiles is visible) we can correct rotation and vertical tilts. After aligning with the laser we can iterate fine adjustments of the bemaline components using SR and laser and also comparing results with the existing beam size monitor.

Using the results of the SRW simulations (already presented in section 2) we made road-map for correcting the main misalignments problems we might face:

Offsets: The offsets don't interfere on the polarized image, except when some aperture is blocking the light, in which case we only loose intensity but the valley-to-peak ration is kept constant (Figure 9a and Figure 9b). We can fix offset issues easily with the alignment laser and introducing orbit bumps.

Horizontal Tilts: In order to correct for horizontal tilts (T_x), we can first used the laser and a pinhole and find the focal plane of the mirror. Changes on the incident angle will change the focal position of the vertical and horizontal plane differently. Using a know source size we can inter ate until both planes re in focus at the same longitudinal position. After we correct using the laser we can optimize this quantity observing the position of minimum separation of the peaks, as shown in Figure 10a, the minimum would indicate we are at the right angle on incidence on the mirror.

Vertical Tilts: To correct for vertical tilts (T_y), we should correct mixing of the horizontal and vertical planes with the laser, since it is a known source it is easier to quantify how far we are from the optimum vertical angle of the mirror. After all the other errors are optimized we should use the polarized synchrotron radiation and move the mirror in order to obtain π-polarized peaks with equal heights.

4 Detailed design - Optical components

The main optical components present in the beamline are listed below and a detailed description of each is given. In order to guarantee a minimum error on the wavefront the optical components have strict requirements. The most important is the surface quality of the mirrors and vacuum window, since these components are further away from the CCD camera and can cause a distortion which will in turn propagate and, in certain circumstances, spoil the image. The requirements on the filters and polarizer are less stringent since they are only centimeters far from the image plane and cannot disturb the almost focused image, too much.

4.1 Toroidal Mirror

According to the simulations presented in section 2, we reached the following final specifications for the toroidal mirror:

- Radius: $R_x = 6592$ mm and $R_y = 5627$ mm
- Radius tolerance: $\leq 0.1\%$ (this gives a maximum variation on the focal plane of 10 mm)
- Incident angle: 22.5^o
- Substrate: SiC (CVD) or Zerodur (or equivalent Sitall CO-115M)
- Coating: SiC or UV protected Aluminum (with Cr binding layer)
- Diameter: 76.2 mm +0/-0.2 mm
- Thickness: 20 ± 3 mm
- Clear aperture: 95-99%
- Surface quality: $\lambda/30$ (λ=632.8 nm over clear aperture) or slope error ≤ 0.25" (rms)
- Roughness: 0.5-0.6 nm
- Waviness pattern: radial or vertically striped

4.2 Plane Mirror

We intent to use a plane mirror from Newport, that is an of-the-shelf component. The main characteristics of this mirror are:

- Substrate: Zerodur
- Coating: UV enhanced aluminium
- Diameter: 76.2 mm +0/-0.13 mm
- Thickness: 14.7 mm $\pm$ 0.25 mm
- Clear Aperture: $\geq$ 80% of diameter
- Surface Quality: $\lambda/20$ (λ=632.8 nm over clear aperture)

4.3 Vacuum Window

The vacuum window is a very special component. It consists of a CF100 flange bonded to an optical flat, specially ordered for this beamline. This new process of bonding, instead of brazing, guarantees that the Fused Silica optical flat retains its surface quality. The main characteristics of the vacuum window are:

- Material: UV - fused silica
- Coating: uncoated
- Diameter: 93.5 mm +0/-0.2 mm
- Thickness: 20.0 mm +0/-0.5 mm
- Clear Aperture: 95% of diameter
- Surface Quality: $\lambda/20$ (λ=632.8 nm over clear aperture)

4.4 Neutral density filters, polarizer and band pass filters

The filters and polarizer are all of-the-shelf components, which can be easily replaced. The main filters and polarizer that will be used are:

- Neutral Density Filter:
  - Material: UV - fused silica
  - Diameter: 50 mm +0/-0.2 mm

  - Thickness: 5 mm +0/-0.1 mm
  - Transmission (%): 50, 25, 10, and 1

- Polarizer:
  - Material: Calcite
  - Coating: uncoated
  - Size (WxHxL): 10 x 25 x 15.9 mm
  - Extinction Ratio: 1/100000

- Band Pass filter:
  - Diameter: 25 mm +0/-0.25 mm
  - Thickness: 3.5 mm
  - Clear aperture: 21 mm
  - Center wavelength: 265 +3.0/-0.0 nm
  - FWHM: 10 nm

- Laser Line filter:
  - Type: Glan-Taylor prism
  - Material: N-BK7
  - Coating: uncoated
  - Diameter: 12.5 mm +0/-0.1 mm
  - Center wavelength: 266 nm
  - FWHM: 1.24 - 2.28 nm

4.5 CCD camera

In the new emittance beamline we will use a set of Ethernet cameras all connected to a PC in the beamline hutch. The cameras are standard PSI measurements cameras (Basler), which makes maintenance simpler. The chosen chipset is a SONY, with a pixel size of 3.75 μm. This is an upgraded version of the CCD cameras already used in the current beamline which will have the same sensibility to the UV region, but higher resolution.

- Type: Basler scA1300-32gm
- Resolution (H/V): 1296 pixels x 966 pixels
- Pixel size: 3.75 μm x 3.75 μm

- Pixel bit depth: 12 bits
- Frame rate: 32 fps
- Sensor: Sony ICX445

5 Detailed design - Mechanical components

In this section we present a more detailed description of two key mechanical elements of the new beam size montior beamline: the finger absorber and the toroidal mirror mount.

5.1 Finger absorber

The finger absorber is a copper piece with 4 mm height and 60 mm length. It is situated upstream of the the first mirror -the toroidal mirror- to protect it from the heat load that would generate the incoming synchrotron radiation. The finger absorber obstructs the mid ± 0.45 mrad on the vertical plane, thus absorbing the radiation in the x-ray range as well as most of the σ-polarized UV light. In total it dissipates 98% of the 240 W of power coming from the dipole and it needs to be water-cooled. This protection is essential to avoid deformations on the mirror surface due to the thermal loads, which could cause severe distortions on the image. Water-cooling the toroidal mirror is not possible for two reasons; due to the special mount on which it will be situated and due to the vibrations of the cooling system which would affect the beam focusing and thus the image detected in the CCD camera.

The technical drawing of the finger absorber of the present beamline is shown in Figure 15, and has similar similar characteristics to the finger absorber planned for the new beamline.

5.2 Mirror mounts

The mount of the toroidal mirror is a gimbal mount, that is, a pivoted support which allows the rotation of the toroidal mirror about the horizontal and vertical axis while keeping fixed the center of the mirror. A photo of a gimbal mount, showing the motor connections and mirror holder is shown in Figure 16.

This type of mount is essential for the toroidal mirror, due to the dependence of the resulting image on the alignment errors. As derived from section 3.2, this piece has to be placed in the beamline with the horizontal radius of the mirror aligned to the central plane of the dipole with an error < 1 mrad. The range of the movements of the mount is of $\pm$ 2.5°, or equivalently $\pm$ 43.6 mrad, with a precision of the order of 1 to 5 μrad, which is enough to position the mirror with respect to the light.

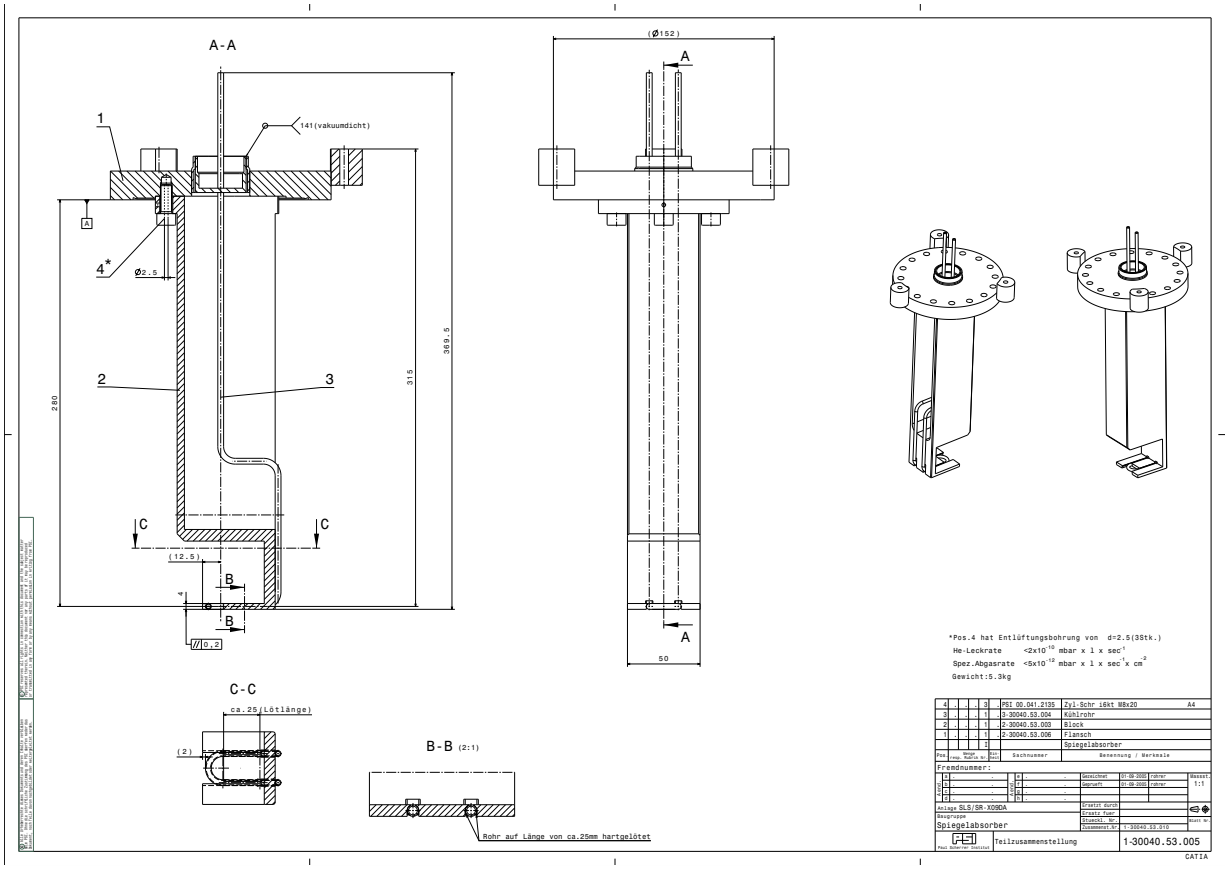

Figure 15: Technical drawing of the finger absorber of the present beamline.

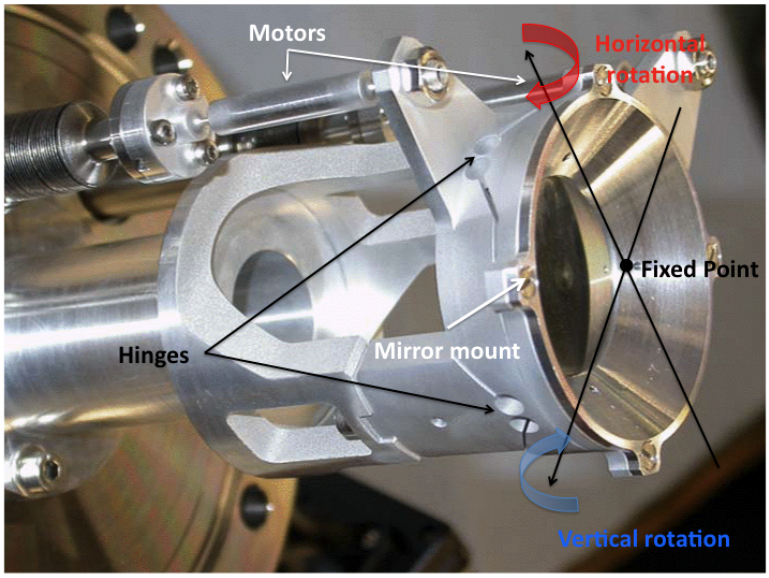

Figure 16: Photo of a PSI gimbal mount, showing the motor connections and mirror holder.

6 Time schedule

- July 2012: Exchange of the absorber in the vacuum chamber of dipole BX08.
- September 2012: Finalize specifications with manufacturer and order the toroidal mirror.
- January 2013: Installation of the vacuum components of the beamline inside the SLS tunnel.
- January - March 2013: Commission of the beamline components.
- March - June 2013: Measurements in the new beamline.

References

[1] Interim report on existing beam instrumentation at the Swiss Light Source storage ring, TIARA-REP-WP6-2011-001

[2] Å. Andersson, M. Böge, A. Lüdeke, V. Schlott and A. Streun, "Determination of a small vertical electron beam profile and emittance at the Swiss Light Source", Nucl. Instrum. Meth. A **591**, 437 (2008).

[3] A. Streun, "Reaching 1 pm vertical emittance at the Swiss Light Source storage ring", TIARA mid-term meeting, CIEMAT, Madrid, June 12-14, 2012.

[4] M. Aiba, M. Böge, N. Milas and A. Streun, Ultra low vertical emittance at SLS through systematic and random optimization, Nuclear Instruments and Methods in Physics Research A, *http://dx.doi.org/10.1016/j.nima.2012.08.012*

[5] T.O. Raubenheimer, "Tolerances to Limit the Vertical Emittance in Future Storage Rings", SLAC-PUB-4937, August 1991.

[6] T. Mitsuhashi, "Measurement of small transverse beam size using interferometry", page 26, DIPAC 2001, ESRF, Grenoble, France.

[7] O. Chubar and P. Elleaume,"Accurate And Efficient Computation Of Synchrotron Radiation In The Near Field Region", proc. of the EPAC98 Conference, 22-26 June 1998, p.1177-1179.

[8] M. Sanchez del Rio and A. Marcelli, "Waviness effects in ray-tracing of real optical surfaces", Nucl. Instrum. Meth. A **319**, 170-177 (1992).